

Out of spuriousity: Improving robustness to spurious correlations without group annotations

Phuong Quynh Le

phuong.le@uni-marburg.de University of Marburg

Jörg Schlötterer

joerg.schloetterer@uni-marburg.de University of Marburg

Christin Seifert

christin.seifert@uni-marburg.de University of Marburg

Abstract

Machine learning models are known to learn spurious correlations, i.e., features having strong relations with class labels but no causal relation. Relying on those correlations leads to poor performance in the data groups without these correlations and poor generalization ability. To improve the robustness of machine learning models to spurious correlations, we propose an approach to extract a subnetwork from a fully trained network that does not rely on spurious correlations. The subnetwork is found by the assumption that data points with the same spurious attribute will be close to each other in the representation space when training with ERM, then we employ supervised contrastive loss in a novel way to force models to unlearn the spurious connections. The increase in the worst-group performance of our approach contributes to strengthening the hypothesis that there exists a subnetwork in a fully trained dense network that is responsible for using only invariant features in classification tasks, therefore erasing the influence of spurious features even in the setup of multi spurious attributes and no prior knowledge of attributes labels.

1 Introduction

Deep neural networks tend to learn spurious attributes, especially when spurious attributes have a positive relation with target labels and are easier to learn which is known as simplicity bias (Shah et al., 2020). This phenomenon leads to the scenario that deep neural networks under-learn invariant information and then lose generalization ability and perform poorly in the data group that does not hold spurious correlations. Spurious features may occur naturally and some of them, such as image background, can be easily detected, whereas other implicit spurious features, such as texture (Geirhos et al., 2018), superficial statistics (Wang et al., 2019) or frequency bias defined by Fourier domain (Wang et al., 2022; 2023) requires more effort. An example of a natural spurious correlation of background is the *cows* and *camels* classification task, where the background *desert* is spuriously correlated with the class *camels* and *grass* positively correlates with *cows* (Beery et al., 2018). These features seem to be easy to learn for deep networks, but relying on them makes networks perform poorly in *minority groups* such as *camels* on *grass* background.

To directly improve the performance of minority groups, mitigation strategies use group label information during training to minimize the worst-group loss (Sagawa et al., 2020a) or re-direct the classification distribution by retraining part of deep networks (Kirichenko et al., 2023). However, group labels can only be collected if one has prior knowledge of the spurious correlations within the dataset, and even in that case, the label annotation process requires much time and effort and might be impossible in a realistic scenario. For example, Wang et al. (2022) defined a frequency shortcut type based on Fourier domain. However, the detection of this type of shortcut is heavily influenced by the order of frequency removal, and their observations are limited to texture-based shortcuts (Wang et al., 2023). To overcome the limitation of collecting group labels, a scope of work leverages hard cases in the training data and defines a weighted

loss for retraining models (Liu et al., 2015; Nam et al., 2020; Zhang et al., 2022; Park et al., 2023). Hard cases are those instances that are misclassified by a model trained with empirical risk minimization (ERM). This definition is based on the assumption that models that are influenced by spurious correlations fail to classify instances where the spurious correlation is not present. However, this assumption is not guaranteed to hold. Further, hard cases are not available in the case of zero training loss, i.e., when the model fully fits the training data. Then, careful early-stopping control is required to obtain a sufficient amount of hard cases without fully deteriorating the ERM training.

To overcome the limitation of the assumption that ERM misclassified instances are hard and spurious-free cases, we propose Pruning Spurious Correlations (**PruSC**) that defines potential spurious groups based on the representation of instances in latent space. Our main motivation is that if the ERM models have spurious correlations, we assume that instances with the same spurious features lie close together in the representation space. That means we can identify groups of instances that have the same spurious feature by applying unsupervised clustering on the output of the penultimate layer. Consequently, to reduce the effect of spurious correlations, we *distort* the clusters of spurious features in feature space. To do that, we introduce a novel application of supervised contrastive loss for training a subnetwork by defining positive and negative anchors based on both target labels and their position in the feature space. By the distortion of spurious feature clusters in representation space, the subnetwork cannot rely on learning and grouping samples based on similar spurious attributes and hence is less influenced by spurious correlations.

PruSC does not require prior knowledge about spurious correlations and is even applicable when more than one spurious attribute is present or the attributes are not trivial for human to annotate (e.g., texture or fluency bias (Geirhos et al., 2018; Wang et al., 2023)). In addition, clusters of spurious attributes form in the representation space as soon as models rely on spurious correlations, i.e., also when models have zero training loss. Hence, our approach to mitigate spurious correlations can be directly applied to a fully trained ERM model

In summary, our contributions are:

- We propose a subnetwork pruning approach PruSC to mitigate the influence of spurious correlations in deep neural networks that does not require group annotations or prior knowledge of spurious features, not even in the validation set for fine-tuning hyper-parameters.
- We propose an effective way to construct contrastive learning batches based on representation clustering.
- Our approach can be applied directly to a trained network without any control requirements (e.g., misclassified cases defined from early stopping).
- Our approach is robust to multiple spurious correlations.

We evaluate our approach on the CelebA dataset (Liu et al., 2015) with potential multiple spurious attributes and the Skin Cancer ISIC dataset (Codella et al., 2019), a realistic image collection used to detect melanoma and an artificial benchmark WaterBird (Sagawa et al., 2020a). Our method outperforms all approaches that do not require group annotations, even for tuning hyper-parameters, and is comparable with methods that require group labels during training. Our code is available at: <https://github.com/pquynhle/spurious-free-subnetwork>

2 Related Work

Robustness to Spurious Correlations. Approaches to mitigate spurious correlations can be broadly classified in two main categories: having prior knowledge of spurious correlations (such as group labels or human annotations) or not having that information.

With full information about spurious correlations on all instances, data-centric approaches like UV-DRO (Srivastava et al., 2020) and LISA (Yao et al., 2022) augment the training data with additional samples to

eliminate the spurious correlation. Group-DRO (Sagawa et al., 2020a) instead utilizes the existing group labels directly to minimize the loss for worst-group performance.

Requiring only a small subset of group labeled training data, BARACK (Sohoni et al., 2022) predicts other instances’ groups and DFR (Kirichenko et al., 2023; Izmailov et al., 2022) retrains part of the model with a small, spurious-free dataset. Prior knowledge of spurious correlations has the advantage that training regimes can directly mitigate undesired attribute influence or relations in the data and consequently yields high accuracy, both on average and in the minority group. However, those group annotations or *human-in-the-loop* annotations are costly and hard to attain in practice. In particular complex spurious attributes, such as fluency bias (Wang et al., 2023) or texture and shape bias (Geirhos et al., 2018) remain challenging, as they are hard to recognize for humans.

When group annotations are not available, (Sohoni et al., 2020; Seo et al., 2022) and Creager et al. (2021) focus on automatically inferring appropriate groups before training a robust model (e.g., Group-DRO) with *pseudo-group labels*. Multiple methods follow a two stage training approach, where the first stage commonly serves to identify hard cases from ERM training. These hard cases are instances that the ERM model fails to classify, presumably because ERM relies on spurious correlations but in those instances the correlation is not present (also called *bias-conflict*). Approaches differ in the second stage: (Liu et al., 2021; Nam et al., 2020) upweight hard cases in an additional training run, while (Yaghoobzadeh et al., 2021) exclusively fine-tune hard cases. CNC (Zhang et al., 2022) and DCWP (Park et al., 2023) utilize the set of hard cases for contrastive learning to define contrastive batches and retrain the whole network (CNC) or to extract a subnetwork (DCWP) with contrastive loss. Different from two-stage methods, DEDIER (Tiwari et al., 2024) uses knowledge distillation to find over-confident predictions in early network layers d then leverages this signal into a graded adjustment of distillation loss on a per-instance level. SELF (LaBonte et al., 2024) finds a small set of hard cases by measuring the degree of disagreement in predictions between an ERM and an early-stopped ERM model, then applies last-layer fine-tuning with this set.

The effectiveness of methods that rely on ERM misclassifications for hard cases depends on both quantity and quality of misclassifications. In cases when ERM models almost perfectly fit the training data (training accuracy close to 100%), there are not enough hard cases (i.e., misclassifications) and these methods fail. To obtain a sufficiently large set of hard cases, careful control of early-stopping regularization or choice of layer d (DEDIER) is required. Hence, those methods can not directly mitigate spurious correlations of a trained ERM model unless trainers have access to the whole training process of that model.

Modular Networks. Modular networks or subnetworks have previously been investigated regarding statistics and connection clusters (Filan et al., 2020). Csordás et al. (2020) proposes a technical training approach for subnetworks in terms of *functional modular*, a subnetwork highly correlated to a designed task. For example, Csordás et al. (2020) investigates whether there exists a subnetwork responsible purely for one class. Using the same technique, Zhang et al. (2021) utilizes the functional modular to solve out-of-distribution generalization by probing subnetworks serving different functional subtasks from a pre-trained ERM.

3 Problem Setting and Example

3.1 Problem Setting

Assume a dataset \mathcal{D} consisting of data samples belonging to groups $g \in \mathcal{G}$ and that the groups have different levels of biases correlated to an input feature of x and the label of y , i.e., a *spurious correlation* (Sagawa et al., 2020b). We set each group $g \in \mathcal{G}$ to be defined by the combination of the label \mathcal{Y} and a corresponding bias attribute \mathcal{A} . Hence, g follows $\mathcal{G} = \mathcal{A} \times \mathcal{Y}$, and we say that there exists a spurious correlation between \mathcal{A} and \mathcal{Y} .

A model trained with ERM on the class labels might be able to separate the classes well but rely on spurious features to do so, resulting in a mismatch between the intended and model-learned solution (Geirhos et al., 2020). Spurious features typically appear in the majority of the dataset. Thus, by using these features, an ERM model can minimize the training loss for the expected average population but still show high errors over the minority group, which lacks these spurious features. Furthermore, in cases where the spurious features

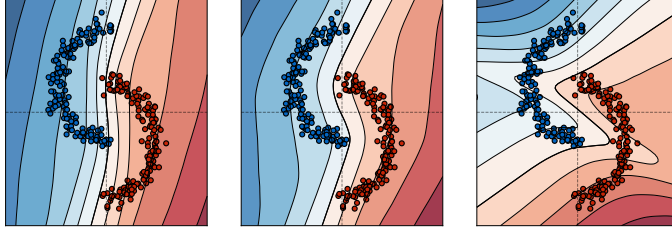


Figure 1: Simple network on the two moons dataset. Decision boundaries (black lines) depend on model capacity and loss. Left: standard ERM with cross-entropy loss with a nearly linear decision boundary and a strong dependence on spurious feature (x-coordinate). Center: Pruned network (masking) using only 50% of the weights at test time shows less dependency on the spurious feature. Right: Masking, and using our contrastive loss (cf. Sec. 5.2.1) results in non-linear decision boundaries with large margins.

are simple to learn (e.g., background instead of the object), ERM prioritizes learning those features over more complex ones and then loses generalization ability. Our goal is to mitigate spurious correlation learning by addressing both, the statistical (highly imbalanced group distributions) and the geometric issues (tendency to learn simpler features).

3.2 Motivating Example

To illustrate the problem and motivate our approach, we revisit a simple 2-D classification task with spurious features (Pezeshki et al., 2021). The two moons dataset \mathcal{D} consists of input pairs (x, y) , where $x = (x_1, x_2) \in \mathbb{R}^2$ and $y \in \{0, 1\}$ (cf. Fig. 1). The dataset contains the artificial direct relation between x_1 and the corresponding label y .

We train three different models on this dataset, showing the effect of i) smaller networks and ii) our contrastive loss formulation (Sec. 5.2.1). A simple feedforward network (5 ReLU layers, 500 hidden units per layer, 100 epochs, cross-entropy loss) can separate the two classes very well (Fig. 1, left). The decision boundary is nearly linear because the cross-entropy loss optimizes for class separation and the model can rely on the correlation between the x-axis values of x and y . We train the same network architecture with random masks (50% of weights in each layer) and use the same fraction of random weights for testing, i.e., we randomly prune the network to 50% of its weights. We observe curved decision boundaries (Fig. 1, center), suggesting that a smaller network within a dense network is less influenced by spurious correlations. Combining masked training and our contrastive loss (Sec. 5.2.1, we obtain a curved decision boundary with a large margin (Fig. 1, right), suggesting that the model uses information from both, the x and y coordinate.

Implications. The above example strengthens two hypotheses for mitigating spurious correlations.

First, **capacity** seems to have an influence. Both, the dense network and the smaller subnetwork with randomly pruned connections perform well on the dataset, but the pruned network has better decision boundaries, i.e., depends less on the spurious feature. However, that does not suggest to train a small architecture from scratch as larger models have a higher ability to learn information and improve performance beyond the bias-variance regime (Nakkiran et al., 2021). Instead, it suggests to first train a large network with large enough capacity to encode all relevant information and then, post-training, extract a subnetwork from it that does not rely on spurious correlation.

The post-training approach also matches our realistic scenario that the existence of spurious correlations becomes evident only after training (and possibly later in the lifetime of a model). Thus, the extraction of a subnetwork without spurious correlations is less expensive than retraining the whole model from scratch. This observation serves as our main motivation.

Second, our **contrastive learning** scheme improves decision boundaries by learning more information from training data than just the simplicity bias features. Our batches of contrastive instances serve as guidance for models to know which feature relations should be less focused on.

4 Background: Subnetwork Extraction

In this section, we outline the approach for the extraction of subnetworks (Csordás et al., 2020). Generally, we aim to extract a sparsely connected subnetwork from a dense network with a binary mask that indicates which weights to include (the subnetwork) and which to discard.

Masking models. Given a trained neural network f , for layer l in L hidden layers of a neural network f , we introduce a learnable parameter $\Pi = (\pi^1, \pi^2, \dots, \pi^L)$ corresponding to each layer’s weights $\mathbf{W} = (\mathbf{w}^1, \mathbf{w}^2, \dots, \mathbf{w}^L)$. Each element of π^l is assumed to be an independent Bernoulli random variable. Each element $\pi_{j,k}^l$ performs as a logit which indicates the probability of keeping the corresponding weight $w_{j,k}^l$. Weight $w_{j,k}^l$ connects the j^{th} -neuron from $(l-1)^{th}$ -layer to k^{th} -neuron from l^{th} -layer, we write each weight and its corresponding logit in short w_i and π_i . During training, network parameters in hidden layers become $(\mathbf{w}^1 \odot \pi^1, \mathbf{w}^2 \odot \pi^2, \dots, \mathbf{w}^L \odot \pi^L)$.

Mask training. To train the binary mask, we freeze the model weights $\mathbf{W} = (\mathbf{w}^1, \mathbf{w}^2, \dots, \mathbf{w}^L)$ and train only the added parameters $\Pi = (\pi^1, \pi^2, \dots, \pi^L)$ with each π_i equal to 0.9 initially, i.e., high keep probability. Modular loss L_{mod} (Csordás et al., 2020) aims to extract a set of sparse weights (the subnetwork) that retain the performance of the original densen network on the classification task.

$$L_{\text{mod}} = L_{\text{CE}} + \alpha \sum_i \pi_i,$$

where L_{CE} is cross-entropy loss, $\sum_i \pi_i$ sparse regularization which keeps a logit π_i small unless it is needed for the task and α is responsible for the strength of the sparse regularization.

The Gumbel-Sigmoid trick (Jang et al., 2017) is applied during training to the logit

$$s_i = \sigma((\pi_i - \log(\log U_1 / \log U_2)) / \tau) \text{ with } U_1, U_2 \sim \text{U}(0, 1),$$

where τ is the temperature and $\sigma(x)$ is the sigmoid function. We obtain the binary mask by

$$m_i = [\mathbb{1}_{s_i > \gamma} - s_i]_{\text{stop}} + s_i$$

where threshold γ is 0.5 by default, $\mathbb{1}$ is the indicator function and $[\cdot]_{\text{stop}}$ is the stop gradient operator.

The final parameters of the resulting subnetwork are defined as $\mathbf{W}' = (\mathbf{w}^1 \odot \mathbf{m}^1, \mathbf{w}^2 \odot \mathbf{m}^2, \dots, \mathbf{w}^L \odot \mathbf{m}^L)$.

5 Our Approach

We hypothesize that instances with the same spurious attribute are nearby in representation space, and that spurious features induce clusters (cf. illustration in Fig.3 A). We verify this hypothesis for multiple attributes on the CelebA dataset (Sec. 5.1).

Our approach centers around two key ideas: First, we identify clusters in the latent space and move instances with the same spurious attributes away from each other and samples of the same class closer to each other. Second, we reduce the representation capacity of the network to a subnetwork that is less prone to spurious correlations.

More specifically, we learn a task-oriented subnetwork (Sec. 5.2) with a task-specific contrastive loss (Sec. 5.2.1) that optimizes the representation space. We detail the specific data selection and sampling procedure for negative and positive samples in the contrastive loss in Sec. 5.2.2. Finally, we present the overall training procedure in Sec. 5.3.

5.1 Analysis of ERM representation space for multiple spurious features

In the presence of spurious features, ERM tends to learn these as predictive features yielding decision boundaries aligned with the spurious feature (as exemplified on the blue moons data set in Fig. 1). We

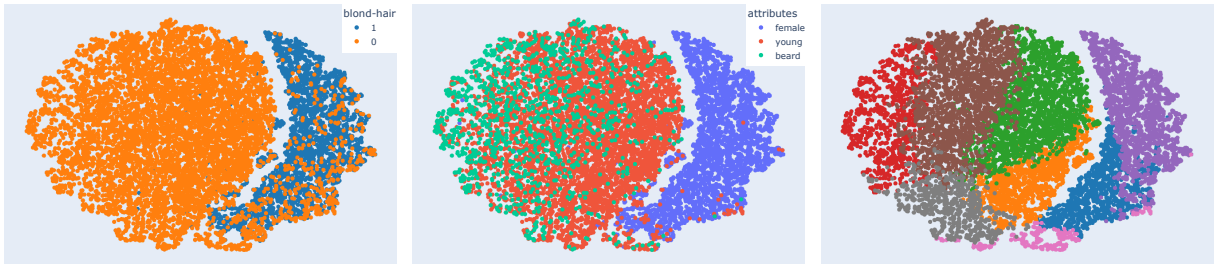


Figure 2: Embedding space (t-SNE) of ERM on CelebA for predicting hair color. Colors represent class labels (left), attributes (center), and k-means cluster labels (right). Spurious attributes are strongly correlated with class labels (e.g., female – blond hair) and sub-manifolds are defined by spurious attributes within a class (non-blond, beard and young). k-means tends to cluster based on attributes with high purity.

analyze the ERM behavior in the presence of multiple spurious features on the CelebA dataset. We use an ERM model for predicting hair color (blond or not blond) having a training accuracy of 95%.

To analyze the feature space, we choose three other attributes (gender, age, presence of a beard) as potential spurious attributes. For a brief description of the CelebA dataset see Sec. 6.1 and Appendix A.1 detailed information. Fig. 2 shows the t-SNE (Van der Maaten & Hinton, 2008) projection of a random subset of CelebA training data representations from the penultimate layer¹. The two classes are well separated in representation space (Fig. 2, left). Interestingly, there is a strong correlation of spurious features and classes in representation space. Female correlates with blond hair, whereas the cluster for non-blond hair (orange cluster, left in Fig. 2) corresponds to young people and people with beard. Moreover, within one class (non-blond hair) the two attributes partition the data in manifolds even though attribute labels are not used during training. Lastly, unsupervised k-means clustering in representation space tends to cluster by attributes with high purity (Fig. 2, right). This means, when optimizing for class separation, instances from the same attribute group $a_i \in \mathcal{A}$ (e.g., persons with beard, young persons) lie close in representation space, even though the group labels are not used during training.

Tab. 1 shows the purity of class (blond or non-blond hair) and spurious attributes (male or female) in clusters obtained from k -means clustering on representations of the CelebA training dataset. Each cluster is assigned a label based on the most frequent class (or spurious) attribute within it. Purity is calculated as the number of correctly matched attribute and cluster labels divided by the total number of instances in that cluster. The table demonstrates that k -means clustering effectively groups samples by class label, but achieves even higher purity for spurious attributes. Fig. 2 (right) demonstrates k -means clustering ($k = 8$) well defines clusters based on not only one but multiple spurious attributes.

The critical case is when the model potentially can separate both, classes and attribute groups, i.e., when the model has high predictive performance **and** the latent space shows clear clusters for spurious features. Such a model will i) make predictions based on spurious features and ii) not generalize well to samples with attribute combinations that do not align with the spurious correlations.

Based on these observations, our goal is to ensure that spurious features do not define data manifolds and cannot be used as discriminative features.

5.2 Task-oriented Subnetwork

To ensure that spurious features do not define data manifolds and cannot be used as discriminative features, we introduce a task-oriented subnetwork, and a contrastive loss that optimizes the representation space. More

Table 1: Purity measurement according to class labels (\mathcal{Y} -purity) and spurious attributes (\mathcal{A} -purity) of unsupervised k -means clustering with different values of k .

k	\mathcal{Y} -purity	\mathcal{A} -purity
4	95.55%	96.48%
8	97.01%	97.32%
16	97.00%	97.80%

¹We discard samples with more than one of the selected attributes for easier interpretation.

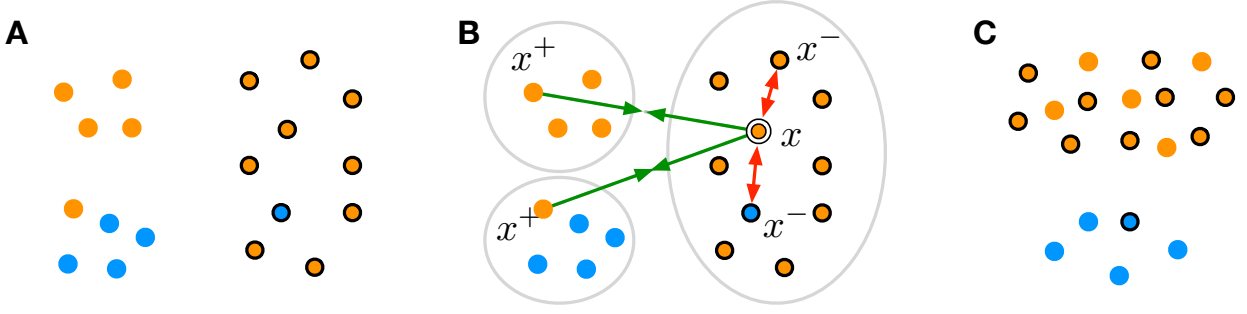


Figure 3: Assumption and overall idea. **A.** Instances from the same class (same colour) lie in different clusters apart in feature space. Instances with the spurious feature (solid border) are nearby in feature space, i.e., the spurious feature induces clusters and primarily defines the shape of the data manifold. **B.** Contrastive loss: For an anchor x , instances from the same class but different clusters constitute positive samples x^+ , instances from the same cluster negative samples x^- . Positive samples are moved closer to the anchor, negative samples away from the anchor. In each iteration multiple samples act as anchors (with their positive and negative samples). **C.** Goal and effect of our contrastive loss. The spurious feature does not define data manifolds and cannot be used as discriminative feature between classes. **Note:** Our approach does not assume (and need) knowledge about the spurious feature.

specifically, we extend the approach for extracting subnetworks (cf. Sec. 4) by incorporating a *task-specific loss* function to prevent the network from learning a grouping of samples based on spurious features. The loss for our task-oriented subnetwork is defined as

$$L = L_{\text{mod}} + \beta L_{\text{task}},$$

where L_{mod} is the modular loss (cf. Sec. 4), L_{task} the task-specific loss, and β is a hyper-parameter to balance loss terms.

The choice of L_{task} in combination with a mask-training dataset $\mathcal{D}_{\text{task}}$ defines the specific task the subnetwork is optimized for. For instance, Csordás et al. (2020) find a subnetwork responsible for a specific class ($\mathcal{D}_{\text{task}}$ contains examples of this class, $L_{\text{task}} = 0$), and Park et al. (2023) identify a subnetwork that is more robust to a spurious feature ($\mathcal{D}_{\text{task}}$ contains instances misclassified by ERM, and L_{task} is a debiasing term). Details on those methods can be found in Appendix A.2. We detail our choice of L_{task} in Sec. 5.2.1 and $\mathcal{D}_{\text{task}}$ in Sec. 5.2.2.

Fig. 3 illustrates the goal and training procedure of our task-oriented subnetwork. Based on the assumption that instances from the same class (same color) lie in different clusters, and that spurious features induce clusters, we define a contrastive loss L_{task} , such that samples from the same class in different clusters are moved closer in representation space, while samples from the same cluster are moved away from each other.

5.2.1 Contrastive Learning

We use a variant of contrastive loss (Khosla et al., 2020) to mitigate the tendency of ERM to form clusters based on spurious attributes. Different from the original work, our contrastive batch is not only defined by class labels, but also by the location of samples in representation space. Fig. 3 outlines the general idea.

For each contrastive batch we randomly sample a set of *anchors* and for each anchor a corresponding set of positive and negative samples. We define positive samples as having the same class as the anchor, but from a different cluster than the anchor. We define negative samples as samples from the same cluster (independent of their class label). For anchor (x, y) belonging to cluster $c \in \mathcal{C}$, the positive set of size P is $\{(x^+, y^+) \mid (x^+, y^+) \in \mathcal{C} \setminus c \wedge y^+ = y\}$ and the negative set of size N is $\{(x^-, y^-) \mid (x^-, y^-) \in c \setminus (x, y)\}$. The contrastive loss term defined with respect to the *anchor* (x, y) is

$$l_{\text{con}}(x) = - \sum_{i=1}^P \log \frac{\exp(z^\top z_i^+ / \tau)}{\sum_P \exp(z^\top z_p^+ / \tau) + \sum_N \exp(z^\top z_n^- / \tau)}$$

where $\tau > 0$ is a scalar temperature hyperparameter, z, z^+, z^- are the normalized representations of corresponding inputs x, x^+ and x^- from *anchor*, *positives* and *negatives* respectively.

This loss forces the representations of samples of the same class across clusters to become more similar and more similar to the *anchor*, while samples representing potential spurious attributes are pushed away from the *anchor*.

5.2.2 Data

PruSC does not require prior knowledge of spurious features and is applicable in the presence of multiple spurious features. We do not assume that group annotations are available but automatically infer groups to construct the de-biasing dataset \mathcal{D}_{task} . Based on the assumption that the representation space of ERM has regions corresponding to spurious attributes (cf. Sec. 5.1, and Fig. 2), we use unsupervised clustering to construct the spurious groups for our dataset \mathcal{D}_{task} .

Given an ERM model, we calculate the embedding of the training data \mathcal{D} and apply k-means clustering on the embedding. Each sample in the training set \mathcal{D} is assigned to a cluster c , $(x, y, c) \in \mathcal{D} = \mathcal{X} \times \mathcal{Y} \times \mathcal{C}$, with input domain \mathcal{X} , class labels \mathcal{Y} , and clusters \mathcal{C} . We define $\mathcal{C} = \{c_j | j \in I\}$ with the cluster index set $j \in I = \{1, 2, \dots, n\}$.

We differentiate clusters based on their class purity. We call a cluster c i -dominant for class i , if at least 90% of its samples belong to class i , i.e., a cluster is class-dominant, if $\exists i \in \mathcal{Y}$ such that $\frac{|\{(x, y, c) \in \mathcal{C} | y=i\}|}{|c|} \geq 0.9$ then c is i -dominant. Otherwise, c is *neutral*. A cluster can be either neutral or i -dominant for some $i \in \mathcal{Y}$ and multiple different clusters may be i -dominant for the same class i . C^i is the union of i -dominant clusters (of the same class i) and C^N is the union of neutral clusters

$$C^i = \bigcup_{j \in I_i} c_j \quad C^N = \bigcup_{j \in I_N} c_j,$$

with $I_i \subset I$ being the set index of i -dominant clusters and $I_N \subset I$ being the set index of neutral clusters.

Let m_i be the minority set of samples with label i assigned to clusters dominated by a different class

$$m_i = \{(x, y, c_j) \mid j \notin (I_i \cup I_N) \wedge y = i\}$$

To construct a class-balanced dataset \mathcal{D}_{task} for subnetwork training, we determine a fixed number p of samples for each class. We draw p samples for class i as follows: First, we take all samples from the minority set m_i . Second, for each cluster in $C^i \cup C^N$, we sample a number of $\frac{p - |m_i|}{|I_i| + |I_N|}$ samples having class label i . We obtain a subset of the training data \mathcal{D}_{task} which is class-balanced with p samples for each class.

5.3 Overall Training Procedure

Given a trained ERM neural network f on dataset \mathcal{D} , we perform the following steps sequentially.

Representation clustering and sub-sampling. First, we extract the representations learned by the ERM model as the output of the last hidden layer of f : f_{emb} . We apply k -means on $f_{emb}(x)$ with a pre-defined k . We determine cluster labels (i -dominant and neutral) and construct the subnetwork mask-training dataset \mathcal{D}_{task} as described in Sec. 5.2.2. In our experiments, we set p , the number of samples for each class such that \mathcal{D}_{task} typically contains 10% of the samples of \mathcal{D} .

Binary mask training. We freeze all weights \mathbf{W} of f and train only the mask $\mathbf{\Pi}$ with the mask-training dataset \mathcal{D}_{task} (cf. Sec. 4). To construct contrastive batches, we randomly sample multiple *anchors* x from distinct cluster together with their corresponding positive x^+ and negative x^- . We accumulate the per-batch contrastive loss by summing over L_{con} of all *anchors* in the batch. The mask $\mathbf{\Pi} = (\pi^1, \pi^2, \dots, \pi^L)$ is updated through the final loss term

$$L = L_{CE} + \alpha \sum_i \pi_i + \beta L_{con},$$

where cross-entropy loss L_{CE} and sparse regularization $\sum_i \pi_i$ correspond to L_{mod} for extracting a sparse subnetwork, and L_{con} is the contrastive loss to mitigate the formation of spurious attribute clusters.

Fine-tuning. After binarization of the trainable mask Π , the resulting binary mask \mathbf{m} defines the parameters of the subnetwork as $\mathbf{W}' = (\mathbf{w}^1 \odot \mathbf{m}^1, \mathbf{w}^2 \odot \mathbf{m}^2, \dots, \mathbf{w}^L \odot \mathbf{m}^L)$. We finetune the extracted subnetwork on the dataset \mathcal{D}_{task} with cross-entropy loss for a few epochs.

6 Experiments

We evaluate the effectiveness of PruSC on three datasets (CelebA, WaterBird, and ISIC) in comparison to state-of-the-art methods (Sec. 6.3). We further examine the impact of PruSC in the presence of multiple potential spurious correlations (Sec. 6.4) and conduct an ablation study for the main components of our approach (Sec. 6.5).

6.1 Datasets

CelebA. Following prior work, our classification target is hair color (blond or non-blond hair) on the CelebA dataset (Liu et al., 2015), where the potential spurious attribute is gender (male or female). Majority groups are blond females and non-blond males with proportions of 44% and 41% of the data. Minority groups are non-blond females (14%) and blond males (1%). We extend the common setup to a multi-spurious dataset by incorporating additional attributes (no beard, young, heavy makeup, wearing lipstick, pale skin) which also pose potential spurious correlations based on their heavily imbalanced distributions.

WaterBird. WaterBird was introduced by Sagawa et al. (2020a) as a standard spurious correlation benchmark. This artificially constructed dataset pastes bird segmentations from the CUB dataset (Wah et al., 2011) onto backgrounds from the Places dataset (Zhou et al., 2018). The birds labeled as either waterbirds or landbirds are placed on backgrounds of either water or land. The task is to classify bird types: $\mathcal{Y} = \{\text{waterbird}, \text{landbird}\}$ and pasting 95% waterbirds on a water background and 95% landbirds on a land background results in spurious correlations in the default training set since models tend to rely on the background instead of actual bird characteristics. Accordingly, the spurious attributes are $\mathcal{A} = \{\text{water background}, \text{land background}\}$.

ISIC. ISIC Skin is a real-world medical dataset provided by the International Skin Imaging Collaboration ISIC (Codella et al., 2019). The objective is to distinguish benign (non-cancerous) cases from malignant (cancerous) cases. Using the source code of Rieger et al. (2020), we retrieved 20,394 images for the two classes benign (17,881) and malignant (2,513) from the ISIC Archive². Nearly half of the benign cases (8,349) have colored patches attached to patients’ skin, whereas no malignant case contains such patches. In this realistic dataset, the group “malignant with patches” is missing from the training set. To create this missing group during the validation procedure, we programmatically add colored patches to a subset of malignant cases outside the area of the lesion, following Nauta et al. (2021).

Additional details about the distribution of datasets with respect to spurious features are provided in Appendix A.1.

6.2 Baselines

Empirical Risk Minimization (ERM) represents conventional training without any procedures for improving worst-group accuracies.

We compare PruSC with two approaches that require group annotations: GroupDRO (Sagawa et al., 2020a) needs knowledge about spurious attributes and group annotations to train from scratch, while DFR (Kirichenko et al., 2023) requires a group-balanced subset for its retraining stage. To meet this requirement in the ISIC dataset, we create artificial samples for the missing group and use those samples during the training of

²<https://www.isic-archive.com/>

Table 2: Performance overview, comparing methods with different assumptions on availability of annotations (A.) of the spurious features in training (Tr) and/or validation set (Val). ** denotes results reported in respective papers, n.a. – results not available in the original paper. * denotes the presence of an artificially created missing group in ISIC, as otherwise DFR and GroupDRO would not be applicable. We **bold** the highest WGA without any group annotation requirement and underline the best among all methods. We report the mean and standard deviation over 5 runs.

w/o A. Tr/Val		CelebA		ISIC		WaterBird	
		AVG	WGA	AVG	WGA	AVG	WGA
✓/✓	ERM (baseline)	90.1±0.3	49.7±1.0	86.9±0.2	34.4±0.8	89.5±0.2	63.3±0.4
✗/✗	DFR	91.3±0.3	88.3±1.1	87.4±1.3*	<u>77.7±2.4*</u>	95.6±0.5	85.6±0.4
✗/✗	GroupDRO	93.0±0.1	88.7±0.3	87.7±0.8*	59.0±0.4*	90.3±0.0	87.0±0.1
✓/✗	CNC**	93.9±0.1	88.9±1.3	n.a.	n.a.	92.0±0.6	89.9±0.6
✓/✗	DEDIER**	93.2±0.06	<u>89.6±1.67</u>	n.a	n.a	92.1±0.39	89.8±0.47
✓/✓	DCWP	88.9±2.3	73.2±2.0	86.4±1.7	45.1±0.8	85.0±0.9	54.8±2.1
✓/✓	DFR _{class}	84.9±2.1	67.7±0.8	74.1±2.6	48.8±6.0	87.5±1.2	74.6±2.9
✓/✓	PruSC	91.0±0.3	<u>89.7±0.3</u>	86.1±0.4	75.1±1.7	90.3±2.2	79.8±0.8

GroupDRO and DFR. To highlight the need of group annotations in DFR, we implement DFR_{class}, which is DFR but uses our automatically inferred class-balanced subset \mathcal{D}_{task} from clustering instead of annotated group-balanced data.

Additionally, we compare to methods with relaxed annotation requirements. CNC (Zhang et al., 2022) and DCWP (Park et al., 2023) work with ERM misclassified cases instead of group annotated samples. These methods sometimes necessitate retraining ERM with early stopping criteria to obtain a sufficiently large set of misclassified samples. DEDIER (Tiwari et al., 2024), is an early readout mechanism with a distillation model. This method identifies misclassified cases from early layers of the network by design. However, DEDIER requires group information during validation to tune hyper-parameters and determine the early layer from which to take the readout.

In contrast to state-of-the-art methods in our comparison, PruSC does not require group annotations at all, neither for (re-)training, nor for fine-tuning hyper-parameters (cf. annotation requirements in the first column of Tab. 2).

DCWP, DFR, DFR_{class} and PruSC, first require an ERM model influenced by spurious correlations before taking actions to mitigate those spurious correlations. For fair comparison, we use the same ERM model which is the ERM baseline reported in Tab. 2 for all methods. Since the training accuracy of this baseline ERM is around 99%, DCWP requires another early stopped model for gathering a sufficient amount of misclassified cases.

Hyper-parameter setup. We use ResNet18 and ResNet50 models pretrained on ImageNet. We train the models for 50 epochs with SGD with a constant learning rate of 10^{-3} , momentum decay of 0.9, weight decay of 10^{-2} , and batch size 32 – 64. All images are resized to 224×224 . We use ResNet50 for the predictive performance evaluation in Tab. 2 to be comparable to the original work for CNC and DEDIER. We use ResNet18 to investigate the robustness of our model to multiple spurious correlations (Sec. 6.4) and in the ablation study (Sec. 6.5). For subnetwork extraction approaches (DCWP and PruSC), we report results with pruning around 50% of the network parameters and discuss the impact of other pruning ratios in Sec. 6.7.

6.3 Predictive Performance

Our main results on predictive performance are shown in Tab. 2. PruSC shows the best performance in terms of worst-group accuracy (WGA) among methods that do not require any group annotations and shows comparable performance in most cases (CelebA and ISIC) to state-of-the-art methods that rely on annotations.

Notably, our method successfully improves the accuracy of the worst group *malignant with patch* in ISIC, although it has never seen an example of that group during training. Our performance is even comparable with GROUPDRO and DFR which explicitly need (artificial) minority group samples during training.

The $\text{DFR}_{\text{class}}$ method mimics DFR but replaces the group-balanced subset (which requires manual annotations) by a class-balanced subset (class annotations are readily available). $\text{DFR}_{\text{class}}$ falls short compared to DFR in all cases by a large margin, highlighting the importance of group annotations in DFR retraining. Using the same retraining dataset as $\text{DFR}_{\text{class}}$, the success of our method PruSC emphasizes the necessity of distorting spurious clusters, which we achieve through a contrastive loss. We empirically analyze the impact of individual components of our method in an ablation study (Sec. 6.5).

While our approach has comparable performance to state-of-the-art on the CelebA and ISIC dataset, it seems to be less effective on the WaterBird dataset. We identified two potential factors, that could explain this behavior. First, the WaterBird dataset has spurious-free validation and test sets, where each class has equal quantities of land and water backgrounds. Therefore, methods that utilize the validation set during training can improve performance without needing explicit group labels. Second, the WaterBird dataset is constructed from 17 bird species divided into two categories: waterbirds and landbirds. Our approach samples a subset $\mathcal{D}_{\text{task}}$ of only around 10% of the training set without access to the bird species information. Consequently, we might lose crucial bird information during sub-sampling, and mask weights containing information that, while irrelevant to the functional task defined on $\mathcal{D}_{\text{task}}$, is essential for recognizing bird types.

6.4 Robustness to Multiple Spurious Correlations

In this section, we analyze how PruSC performs in the presence of multiple spurious correlations within a dataset. Since we do not explicitly use information about the spurious attribute during subnetwork training, we expect the representations to be agnostic to any spurious feature. We use the CelebA dataset which has a potential set of spurious attributes \mathcal{A} (Seo et al., 2022) (for details see Appendix A.3). Specifically, we investigate six potential spurious attributes $a_i \in \mathcal{A} = \{\text{male, presence of beard, heavy makeup, wearing lipstick, young, pale skin}\}$. For each attribute a_i , we create a group set $\mathcal{G} = \{(\text{blond}, a_i), (\text{non-blond}, a_i), (\text{blond}, \text{non-}a_i), (\text{non-blond}, \text{non-}a_i)\}$. We train an ERM model to predict hair color and evaluate performance separately for each group in \mathcal{G} . We then train all methods for correcting spurious attributes. GroupDRO and DFR are trained on balanced groups for the attribute male.³

6.4.1 Evaluation Metrics

We report **worst-group accuracy (WGA)** for each spurious attribute a_i evaluated on groups in \mathcal{G} . WGA is the standard metric to evaluate whether models use spurious correlations. A significant drop between average accuracy and worst-group accuracy is a strong indicator of relying on spurious correlations. To assess the impact on the group with the fewest training samples (usually the group with a spurious attribute uncorrelated to a target label), we report **minority-group accuracy (MGA)** for each spurious attribute a_i . To assess group fairness, i.e., whether all groups have similar prediction error, we measure the **unbiased accuracy gap (UAG)**. Unbiased accuracy (UA) is the accuracy on a balanced test set, sampled such that there is no correlation between the attribute a_i and a target label. UGA is the difference of the overall (official) test set accuracy and UA. A small UAG indicates that groups are treated equally, regardless of their distribution in the dataset.

6.4.2 Results

The ERM models usually fail for the minority group represented by target and uncorrelated attributes. For example, for the attribute gender = male, the ERM model only has 50.2% accuracy for the group (blond hair, male) since in the training set there are only 1,102 samples in the group (blond hair, male) while the group (non-blond hair, male) contains 53,483 samples. In all of these cases, the accuracy for the minority group is the worst-group accuracy evaluated by the baseline ERM model.

³GroupDRO and DFR are single-attribute methods, and cannot be trained for multiple attributes at the same time. Since the spurious attributes in CelebA are themselves strongly correlated (male, beard) there are still performance improvements for attribute groups not specifically trained for.

Table 3: **Minority group** accuracy across multiple spurious attributes in CelebA. Each method train with CelebA with target $\mathcal{T} = \{\text{blond hair}\}$, spurious attributes set are $\mathcal{A} = \{\text{male (M)}, \text{no beard (NB)}, \text{heavy makeup (HM)}, \text{wearing lipstick (WL)}, \text{young (Y)}, \text{pale skin (PS)}\}$. GroupDRO and DFR train extensively for attribute $a_i = \text{M}$ while ERM (baseline), DCWP, and Ours only train with target label information. We report the performances of the minority groups defined in the training set - those groups are aligned with the worst-group defined by ERM worst-group accuracy. We **bold** the largest increase from the baseline among all methods.

w/o A. Tr/Val		M	NB	HM	WL	Y	PS
✓/✓	ERM (baseline)	50.2	37.5	79.6	79.4	87.5	83.5
✗/✗	GroupDRO	88.8	85.9	90.6	89.9	91.3	87.5
✗/✗	DFR	85.6	78.1	83.1	82.6	85.4	81.9
✓/✓	DCWP	81.8	78.1	76.9	76.9	83.7	79.2
✓/✓	PruSC	91.2	92.2	92.7	92.2	92.8	88.7

In Tab. 3, we report the performance of the minority group across multiple spurious attributes. The details of data distribution are shown in Tab. 7 and the full details for group accuracy of the groups $\mathcal{G} = \{(\text{blond}, a_i), (\text{non-blond}, a_i), (\text{blond}, \text{non-}a_i), (\text{non-blond}, \text{non-}a_i)\}$ in Tab. 9) (Appendix).

Tab. 3 shows that PruSC has the largest improvement from the baseline in all spurious attribute cases. Especially in the case of the spurious feature “male”, PruSC performs better than GroupDRO or DFR which are trained with known group labels for this attribute.

The worst-group accuracy of baselines ERM, using group labels GroupDRO and PruSC not using prior knowledge of spurious attributes are reported in Tab. 4 (WGA).

The increase in worst-group accuracy (WGA) compared to the baselines suggests that all methods are able to unlearn certain biased features. However, in a realistic dataset, e.g. CelebA, there are identical distributions in the train and official test set a model can use to obtain high accuracy on the majority group, but fail on other groups. Therefore, measuring WGA on the official test set can prove that the methods decrease the impact of bias features, but can not tell to what extent the model treats all groups equally. Tab. 4 shows that our approach is on par with GroupDRO in UA and WGA. This indicates that both methods can effectively unlearn spurious correlations and maintain strong performance even when there is a distribution shift from a highly imbalanced training set to a balanced test set. However, PruSC shows a smaller UGA in all cases and is, therefore, more consistent among different spurious attributes and shows a more balanced performance among groups.

Table 4: Multi-attributes. The table reports unbiased accuracy (UA), worst-group accuracy (WGA) and unbiased accuracy gap (Gap) - the gap between average and corresponding unbiased accuracy. We **bold** the highest WGA and underline the smallest Gap for each spurious attribute. The \uparrow indicates the higher the better and the \downarrow indicates the lower the better.

	ERM			GroupDRO			PruSC		
	UA \uparrow	WGA \uparrow	UAG \downarrow	UA \uparrow	WGA \uparrow	UAG \downarrow	UA \uparrow	WGA \uparrow	UAG \downarrow
male	81.6	50.2	7.8	90.7	88.5	2.2	90.5	89.6	<u>0.4</u>
no beard	79.8	37.5	9.6	90.9	85.9	2.0	91.0	89.6	<u>0.9</u>
heavy makeup	90.1	79.6	0.7	91.4	89.4	1.5	90.2	88.9	<u>0.1</u>
wearing lipstick	88.8	79.4	0.6	90.9	89.6	2.0	90.1	88.7	<u>0.0</u>
young	91.8	87.5	2.4	91.0	84.5	1.9	89.3	81.4	<u>0.8</u>
pale skin	91.4	83.5	2.0	90.8	87.5	2.1	89.8	88.7	<u>0.3</u>

Table 5: Ablation study on CelebA dataset (target: blond hair, spurious attribute: male). Effect of pruning (Pr) and finetuning (Ft) steps with (\checkmark) and without (\times) our contrastive loss. \checkmark_{last} means finetuning on the last layer only.

Setting	Pruning	Fine-tuning	ConLoss Pr	ConLoss Ft	WGA	AVG	UA
1 (PruSC)	\checkmark	\checkmark	\checkmark	\times	89.6	90.1	90.5
2	\checkmark	\checkmark	\checkmark	\checkmark	67.7	83.7	80.4
3	\checkmark	\checkmark	\times	\times	41.8	91.5	73.9
4	\checkmark	\times	\checkmark	\times	43.7	89.6	74.4
5	\times	\checkmark	\times	\checkmark	67.4	88.8	81.6
6	\times	\checkmark	\times	\times	78.9	87.9	87.2
7 (DFR _{class})	\times	\checkmark_{last}	\times	\times	79.5	83.8	85.5

6.5 Ablation study

Tab. 5 shows an overview of our ablations: performing the pruning and fine-tuning steps, with and without our contrastive loss, respectively (ConLoss Pr, ConLoss Ft).

Contrastive Loss. Settings 1 and 2 demonstrate the impact the contrastive loss during fine-tuning (ConLoss Ft) when training a subnetwork. Similarly, settings 5 and 6 show the influence of contrastive loss while not pruning but only fine-tuning the whole network with \mathcal{D}_{task} . In both cases, using the contrastive loss in fine-tuning downgrades the performance. Setting 3 reveals that without contrastive loss in the training mask (ConLoss Pr), the WGA drops significantly (89.6% from setting 1 to 41.8% in setting 3). It shows that our final combination (only using contrastive loss during pruning) is the best combination and surpasses other combinations by large margins. In other words, our defined contrastive loss is most effective when applied to the mask training instead of directly to the model weight training. The contrastive loss forces the pruning process to retain only the connections that contribute to an optimized representation, ensuring that all spurious attributes are distributed in the representation space. Furthermore, in the pruning stage, the backpropagation process only updates the masks, which later will be binarized by Gumbel-Sigmoid, instead of directly updating the model weights.

Fine-tuning. Without fine-tuning (setting (4)) the performance drops significantly. Without fine-tuning the model on the dataset \mathcal{D}_{task} , the subnetwork’s performance is similar to that before pruning. Note, that we only need to finetune 2 – 5 epochs. This finding matches with previous work on modular subnetworks (Csordás et al., 2020; Zhang et al., 2021; Park et al., 2023) that require retraining or fine-tuning the remaining network after pruning to achieve better performance.

Subnetwork. The three ablation experiments (settings (5) to (7)) answer the question of whether one can improve the worst-group accuracy only by fine-tuning and getting advantages from the design of a class-balanced subset. We either fine-tune the whole network (setting (5) and (6)), or only one last layer (setting (7)) for same number of epochs. The latter setting is equivalent to DFR_{class}, with \mathcal{D}_{task} . We observe no significant improvement when fine-tuning the whole network compared to fine-tuning only the last layer (setting 6 vs. 7), fine-tuning the whole network even results in worse WGA. As noted before, using the contrastive loss during fine-tuning again drops the group-worst accuracy.

6.6 Variant of contrastive learning.

We study the effectiveness of our choices for contrastive batch learning in PruSC. Results reported in Tab. 6 shows that other ablations of contrastive batch are less effective than our choice in terms of improvement worst-group accuracy. Recall our default setting: sampling a random *anchor*, *positives* are defined by samples taking from different clusters and having the same class label with the *anchor*, while *negatives* are defined by samples from the same cluster with the *anchor*.

We ablate the negative choice by keeping *anchor* and *positives* the same as default while *negatives* are chosen by the same cluster and different class label (Neg. Ablation). The effectiveness of this variant is affected by the purity of clusters. As shown in Fig. 2 and Tab. 1, k -means clustering on train representation of a convergent model can lead to high purity clusters in terms of class labels; therefore, by choosing different class *negatives*, we either lacking negative samples for contrastive learning or an early-stopping models is required to get more negative samples which we want to avoid. We also compare our choice to the classic SupCon (Khosla et al., 2020), i.e., *positives* and *negatives* are defined only by class labels. SupCon does not work since it aims to tighten samples within one cluster which has a high potential of having the same spurious features. Furthermore, SupCon only helps to separate classes, which ERM models in some cases do already well enough (cf. Fig. 2, left and Fig. 5, left). Our contrastive batch is defined not only by class labels like in SupCon but also by the positions of samples in the representation space based on clustering.

6.7 The impact of pruning ratio.

Fig. 4 shows the average and worst-group accuracy evaluated on the CelebA dataset with respect to different pruning ratios. We consider the set up of classifying blond hair and spurious feature is male or not-male. While the average accuracy does not change much as long as the pruning ratio is under 70%, the worst-group accuracy varies more significantly. The smaller gap between the average and worst-group accuracy indicates that the models are less prone to spurious correlations. In the CelebA dataset, the most effective pruning ratio is around 40% to 50%. When pruning beyond 70% of the parameters, the models seem to fail to predict accurately, as both the worst-group and average accuracy drop.

7 Feature visualization

In this section, we discuss how PruSC affects the representation space at the end. We show in the previous part that ERM tends to learn and cluster samples based on spurious attributes during training (Fig. 2). In Fig. 5 (left), we visualize the embedding space of the non-blond hair class in the test set of the same ERM model, which reveals again ERM learns based on spurious features. Despite achieving high average test accuracy (90%), the fact that ERM learns to use spurious features for predicting leads to low worst-group accuracy (49.7%) and lack of generalization ability.

DCWP mitigates spurious correlations by extracting a subnetwork by training a contrastive loss, and sampling positives and negatives from bias-conflict (ERM misclassified) and bias-align (ERM correctly classified) cases. From the predictive result, DCWP successfully improves the worst-group accuracy (73%), however, the model still tends to group samples by female attribute (Fig. 5, center). We hypothesize that defining bias-conflict based on ERM misclassified cases is not reliable. When a spurious attribute (female) is easy to learn and strongly correlated with a class (non-blond hair), the model easily learns and predicts correctly based on the spurious feature, even in the early stage of training.

PruSC eliminates this reliance on spurious feature learning. While average accuracy remains high (91%) through cross-entropy loss, the use of contrastive learning within clusters makes the learning spurious process

Table 6: Average accuracy (AVG) and worst-group accuracy (WGA) of models trained on CelebA dataset with different choices of contrastive batch.

	AVG	WGA
Default	91.0%	89.7%
Neg. Ablation	90.2%	73.1%
SupCon	92.2%	61.5%

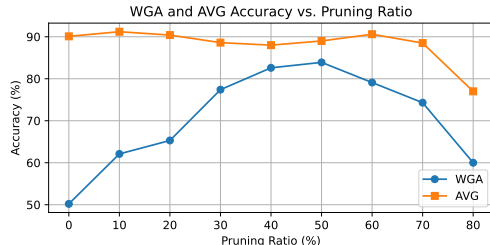


Figure 4: Worst-group accuracy (WGA) and average accuracy (AVG) of CelebA according to pruning ratio.

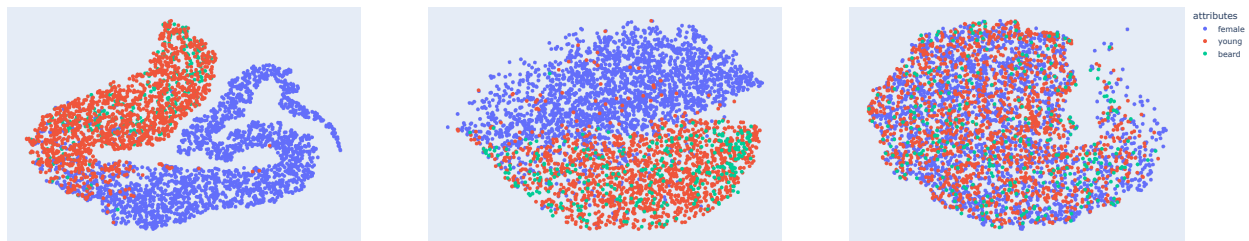


Figure 5: The test set embedding space of ERM (left), DCWP (center) and PruSC (right) on CelebA for predicting blond hair color. We visualize the class of non-blond hair with colors representing three spurious attributes: female, young, and beard. All models achieve high average test accuracy (over 88%, see Tab. 2). However, while ERM and DCWP cluster samples by spurious attributes, our PruSC mixes samples with these attributes, resulting in better worst-group accuracy.

harder, thus, improving the generalization. Our pruned model mixes up samples with different attributes within one class showing its independence on these spurious attributes (Fig. 5, right).

In our visualization, we use the official train and test split of CelebA where multiple spurious correlations are possible but not exposed with high spuriousness. We expect the phenomenon can be shown more concretely in the case of synthetic data constructed to have high spurious correlations. More visualizations are shown in Appendix A.4.

8 Conclusion

In this paper, we presented PruSC to extract a spurious-free subnetwork from a fully trained neural network. We do not require annotations of spurious features, but instead, optimize the representation space to uncorrelated spurious attributes and class labels by forcing examples of the same class which is in different clusters (presumably due to different spurious attributes) to become more similar. PruSC achieves competitive worst-group accuracy across several benchmarks *without* requiring annotations of the spurious feature(s). We find that this not only reduces annotation overhead and makes the method applicable in cases where spurious attributes are not known beforehand, but also results in models that are robust to multiple spurious correlations.

Notably, we extract the subnetwork from a fully trained network without extensively retraining the weights. This shows that even when models are heavily influenced by spurious correlations, there exists a smaller part of the network that learns the invariant features relevant to the task. This finding is a promising direction for future research.

One limitation of our pruning method is that it fails to explicitly explain the exact roles of the pruned connections. It is possible that the pruned connections encode some information essential for the classification task but not defined during pruning. This potential missing information could be crucial for effectively learning the WaterBird dataset, as discussed in Sec.6.3.

References

- Sara Beery, Grant Van Horn, and Pietro Perona. Recognition in terra incognita. In *Proceedings of the European conference on computer vision (ECCV)*, pp. 456–473, 2018.
- Noel Codella, Veronica Rotemberg, Philipp Tschandl, M. Emre Celebi, Stephen Dusza, David Gutman, Brian Helba, Aadi Kalloo, Konstantinos Liopyris, Michael Marchetti, Harald Kittler, and Allan Halpern. Skin Lesion Analysis Toward Melanoma Detection 2018: A Challenge Hosted by the International Skin Imaging Collaboration (ISIC), 2019.
- Elliot Creager, Jörn-Henrik Jacobsen, and Richard Zemel. Environment inference for invariant learning. In *International Conference on Machine Learning*, pp. 2189–2200. PMLR, 2021.
- Róbert Csordás, Sjoerd van Steenkiste, and Jürgen Schmidhuber. Are Neural Nets Modular? Inspecting Functional Modularity Through Differentiable Weight Masks. In *International Conference on Learning Representations*, 2020.
- Daniel Filan, Shlomi Hod, Cody Wild, Andrew Critch, and Stuart Russell. Pruned neural networks are surprisingly modular. *arXiv preprint arXiv:2003.04881*, 2020.
- Robert Geirhos, Patricia Rubisch, Claudio Michaelis, Matthias Bethge, Felix A Wichmann, and Wieland Brendel. Imagenet-trained CNNs are biased towards texture; Increasing shape bias improves accuracy and robustness. In *International Conference on Learning Representations*, 2018.
- Robert Geirhos, Jörn-Henrik Jacobsen, Claudio Michaelis, Richard Zemel, Wieland Brendel, Matthias Bethge, and Felix A Wichmann. Shortcut learning in deep neural networks. *Nature Machine Intelligence*, 2(11): 665–673, 2020.
- Pavel Izmailov, Polina Kirichenko, Nate Gruver, and Andrew G Wilson. On feature learning in the presence of spurious correlations. *Advances in Neural Information Processing Systems*, 35:38516–38532, 2022.
- Eric Jang, Shixiang Gu, and Ben Poole. Categorical reparameterization with gumbel-softmax. In *International Conference on Learning Representations*, 2017.
- Prannay Khosla, Piotr Teterwak, Chen Wang, Aaron Sarna, Yonglong Tian, Phillip Isola, Aaron Maschiot, Ce Liu, and Dilip Krishnan. Supervised contrastive learning. In *Advances in neural information processing systems*, volume 33, pp. 18661–18673, 2020.
- Polina Kirichenko, Pavel Izmailov, and Andrew Gordon Wilson. Last Layer Re-Training is Sufficient for Robustness to Spurious Correlations. In *The Eleventh International Conference on Learning Representations*, 2023.
- Tyler LaBonte, Vidya Muthukumar, and Abhishek Kumar. Towards Last-layer Retraining for Group Robustness with Fewer Annotations. In *Advances in Neural Information Processing Systems*, volume 36, 2024.
- Evan Z Liu, Behzad Haghgoo, Annie S Chen, Aditi Raghunathan, Pang Wei Koh, Shiori Sagawa, Percy Liang, and Chelsea Finn. Just Train Twice: Improving Group Robustness without Training Group Information. In Marina Meila and Tong Zhang (eds.), *Proceedings of the 38th International Conference on Machine Learning*, volume 139 of *Proceedings of Machine Learning Research*, pp. 6781–6792. PMLR, 18–24 Jul 2021.
- Ziwei Liu, Ping Luo, Xiaogang Wang, and Xiaoou Tang. Deep learning face attributes in the wild. In *Proceedings of the IEEE international conference on computer vision*, pp. 3730–3738, 2015.
- Preetum Nakkiran, Gal Kaplun, Yamini Bansal, Tristan Yang, Boaz Barak, and Ilya Sutskever. Deep double descent: Where bigger models and more data hurt. *Journal of Statistical Mechanics: Theory and Experiment*, 2021(12):124003, 2021.
- Junhyun Nam, Hyuntak Cha, Sungsoo Ahn, Jaeho Lee, and Jinwoo Shin. Learning from failure: De-biasing classifier from biased classifier. *Advances in Neural Information Processing Systems*, 33:20673–20684, 2020.

-
- Meike Nauta, Ricky Walsh, Adam Dubowski, and Christin Seifert. Uncovering and correcting shortcut learning in machine learning models for skin cancer diagnosis. *Diagnostics*, 12(1):40, 2021.
- Geon Yeong Park, Sangmin Lee, Sang Wan Lee, and Jong Chul Ye. Training Debiased Subnetworks With Contrastive Weight Pruning. In *Proceedings of the IEEE/CVF Conference on Computer Vision and Pattern Recognition*, pp. 7929–7938, 2023.
- Mohammad Pezeshki, Oumar Kaba, Yoshua Bengio, Aaron C Courville, Doina Precup, and Guillaume Lajoie. Gradient starvation: A learning proclivity in neural networks. In *Advances in Neural Information Processing Systems*, volume 34, pp. 1256–1272, 2021.
- Laura Rieger, Chandan Singh, W. James Murdoch, and Bin Yu. Interpretations Are Useful: Penalizing Explanations to Align Neural Networks with Prior Knowledge. In *Proceedings of the 37th International Conference on Machine Learning*, pp. 11. JMLR.org, 2020.
- Shiori Sagawa, Pang Wei Koh, Tatsunori B. Hashimoto, and Percy Liang. Distributionally Robust Neural Networks. In *International Conference on Learning Representations*, 2020a.
- Shiori Sagawa, Aditi Raghunathan, Pang Wei Koh, and Percy Liang. An investigation of why overparameterization exacerbates spurious correlations. In Hal Daumé III and Aarti Singh (eds.), *Proceedings of the 37th International Conference on Machine Learning*, volume 119 of *Proceedings of Machine Learning Research*, pp. 8346–8356. PMLR, 13–18 Jul 2020b.
- Seonguk Seo, Joon-Young Lee, and Bohyung Han. Unsupervised learning of debiased representations with pseudo-attributes. In *Proceedings of the IEEE/CVF Conference on Computer Vision and Pattern Recognition*, pp. 16742–16751, 2022.
- Harshay Shah, Kaustav Tamuly, Aditi Raghunathan, Prateek Jain, and Praneeth Netrapalli. The pitfalls of simplicity bias in neural networks. In *Advances in Neural Information Processing Systems*, volume 33, pp. 9573–9585, 2020.
- Nimit Sohoni, Jared Dunnmon, Geoffrey Angus, Albert Gu, and Christopher Ré. No subclass left behind: Fine-grained robustness in coarse-grained classification problems. In *Advances in Neural Information Processing Systems*, volume 33, pp. 19339–19352, 2020.
- Nimit Sharad Sohoni, Maziar Sanjabi, Nicolas Ballas, Aditya Grover, Shaoliang Nie, Hamed Firooz, and Christopher Re. BARACK: Partially Supervised Group Robustness With Guarantees. In *ICML 2022: Workshop on Spurious Correlations, Invariance and Stability*, 2022.
- Megha Srivastava, Tatsunori Hashimoto, and Percy Liang. Robustness to spurious correlations via human annotations. In *International Conference on Machine Learning*, pp. 9109–9119. PMLR, 2020.
- Rishabh Tiwari, Durga Sivasubramanian, Anmol Mekala, Ganesh Ramakrishnan, and Pradeep Shenoy. Using Early Readouts to Mediate Featural Bias in Distillation. In *Proceedings of the IEEE/CVF Winter Conference on Applications of Computer Vision*, pp. 2638–2647, 2024.
- Laurens Van der Maaten and Geoffrey Hinton. Visualizing data using t-SNE. *Journal of machine learning research*, 9(11), 2008.
- Catherine Wah, Steve Branson, Peter Welinder, Pietro Perona, and Serge Belongie. The caltech-ucsd birds-200-2011 dataset. *California Institute of Technology*, 2011.
- Haohan Wang, Zexue He, Zachary C Lipton, and Eric P Xing. Learning robust representations by projecting superficial statistics out. In *International Conference on Learning Representations*, 2019.
- Shunxin Wang, Raymond Veldhuis, Christoph Brune, and Nicola Strisciuglio. Frequency shortcut learning in neural networks. In *NeurIPS 2022 Workshop on Distribution Shifts: Connecting Methods and Applications*, 2022.

-
- Shunxin Wang, Raymond Veldhuis, Christoph Brune, and Nicola Strisciuglio. What do neural networks learn in image classification? A frequency shortcut perspective. In *Proceedings of the IEEE/CVF International Conference on Computer Vision*, pp. 1433–1442, 2023.
- Yadollah Yaghoobzadeh, Soroush Mehri, Remi Tachet des Combes, Timothy J Hazen, and Alessandro Sordani. Increasing Robustness to Spurious Correlations using Forgettable Examples. In *Proceedings of the 16th Conference of the European Chapter of the Association for Computational Linguistics: Main Volume*, pp. 3319–3332, 2021.
- Huaxiu Yao, Yu Wang, Sai Li, Linjun Zhang, Weixin Liang, James Zou, and Chelsea Finn. Improving out-of-distribution robustness via selective augmentation. In *International Conference on Machine Learning*, pp. 25407–25437. PMLR, 2022.
- Dinghuai Zhang, Kartik Ahuja, Yilun Xu, Yisen Wang, and Aaron Courville. Can subnetwork structure be the key to out-of-distribution generalization? In *International Conference on Machine Learning*, pp. 12356–12367. PMLR, 2021.
- Michael Zhang, Nimit S Sohoni, Hongyang R Zhang, Chelsea Finn, and Christopher Ré. Correct-N-Contrast: a Contrastive Approach for Improving Robustness to Spurious Correlations. In *International Conference on Machine Learning*, pp. 26484–26516. PMLR, 2022.
- Bolei Zhou, Agata Lapedriza, Aditya Khosla, Aude Oliva, and Antonio Torralba. Places: A 10 Million Image Database for Scene Recognition. *IEEE Transactions on Pattern Analysis and Machine Intelligence*, 40(6): 1452–1464, 2018. doi: 10.1109/TPAMI.2017.2723009.

A Appendix / supplemental material

A.1 Datasets

CelebA. Tab. 7 shows the distribution of group $\mathcal{G} = \{(\text{blond}, a_i), (\text{non-blond}, a_i), (\text{blond}, \text{non-}a_i), (\text{non-blond}, \text{non-}a_i)\}$ in training dataset and testing dataset. This shows the imbalanced distribution of the group (target, correlated attribute) and (target, un-correlated attribute). The models can both depend on the easier to learn features and the dominance of training data to suffer from spurious correlations. Generally, the minority group (group having smallest portion in training set) is the group having worst accuracy in test (with respect to baseline ERM).

Table 7: Data distribution in CelebA dataset of groups $g \in \mathcal{G} = \mathcal{Y} \times \mathcal{A}$ forming by target class blond or non-blond hair $y \in \mathcal{Y}$ and spurious attribute $a \in \mathcal{A}$. Gray color highlights the **minority group** - smallest $p(g)$ among groups in the training set.

Attribute a	Group g	Training distribution			Testing distribution		
		Quantity	$p(g)$ (%)	$p(t a)$ (%)	Quantity	$p(g)$ (%)	$p(t a)$ (%)
male (M)	$y = 0, a = 0$	1,558	2.1	7.8	14,415	44.3	76.4
	$y = 0, a = 1$	53,483	71.7	98.0	13,391	41.1	97.9
	$y = 1, a = 0$	18,417	24.7	92.2	4,463	13.7	23.6
	$y = 1, a = 1$	1,102	1.5	2.0	285	0.9	2.1
no beard (NB)	$y = 0, a = 0$	21,229	28.5	98.9	5,369	16.5	98.8
	$y = 0, a = 1$	33,812	45.3	63.7	22,437	68.9	82.7
	$y = 1, a = 0$	243	0.3	1.1	64	0.2	1.2
	$y = 1, a = 1$	19,276	25.9	36.3	4,684	14.4	17.3
heavy makeup (HM)	$y = 0, a = 0$	53,885	72.3	89.5	18,620	57.2	92.3
	$y = 0, a = 1$	1,156	1.6	8.1	9,186	28.2	74.2
	$y = 1, a = 0$	6,317	8.5	10.5	1,550	4.8	7.7
	$y = 1, a = 1$	13,202	17.7	91.9	3,198	9.8	25.8
wearing lipstick (WL)	$y = 0, a = 0$	53,480	71.7	93.6	16,386	50.3	94.9
	$y = 0, a = 1$	1,561	2.1	9.0	11,420	35.1	74.7
	$y = 1, a = 0$	3,678	4.9	6.4	880	2.7	5.1
	$y = 1, a = 1$	15,841	21.2	91.0	3,868	11.9	25.3
young (Y)	$y = 0, a = 0$	16,262	21.8	31.4	6,473	19.9	89.2
	$y = 0, a = 1$	3,257	4.4	14.3	21,333	65.5	84.3
	$y = 1, a = 0$	35,456	47.6	68.6	780	2.4	10.8
	$y = 1, a = 1$	19,585	26.3	85.7	3,968	12.2	15.7
pale skin (PS)	$y = 0, a = 0$	53,664	72.0	74.7	26,758	82.2	85.8
	$y = 0, a = 1$	1,377	1.8	49.9	1,048	3.2	76.1
	$y = 1, a = 0$	18,139	24.3	25.3	4,418	13.6	14.2
	$y = 1, a = 1$	1,380	1.9	50.1	330	1.0	23.9

WaterBird. WaterBird is an artificial dataset generated based on the code from (Sagawa et al., 2020a). Similar to the CelebA dataset, the training set of WaterBird suffers from both high class imbalance and significant spurious correlations, with waterbirds typically appearing in water backgrounds and landbirds in land backgrounds. Interestingly, the validation and test sets of WaterBird are balanced in terms of these spurious correlations, with equal numbers of waterbirds and landbirds appearing in both land and water backgrounds. Therefore, we expect that all methods tuning hyperparameters on the validation set will have access to distribution information reflective of the test set, leading to high overall performance and improved worst-group accuracy. We show details number of samples in each group in Tab. 8.

Table 8: Distribution of samples in dataset WaterBird and ISIC. Gray color highlights the minority group. WaterBird has similar distribution between validation and test sets, and they are both spurious-free within a class (i.e., equal number of samples with land or water background). In ISIC, we construct a group balanced validation set for the purpose of training DFR which requires a held-out group-balanced dataset.

Dataset	Groups	Train	Validation	Test
WaterBird	waterbird on water	1057	133	642
	waterbird on land	56	133	642
	landbird on water	184	466	2255
	landbird on land	3498	467	2255
ISIC	Benign with patch	5526	60	2763
	Benign without patch	6314	60	3158
	Malignant with patch	0	60	821
	Malignant without patch	1571	60	821

A.2 Task-oriented Subnetworks

Csordás et al. (2020) aims to highlight sets of non-shared weights solely responsible for individual class k by training a mask with class k removed from the training dataset ($\mathcal{C}_{task} = \mathcal{D} \setminus \{(x, y | y = k)\}$) and need not add any other loss term. The weights solely responsible for this class will be absent from the resulting mask. Results show that the performance of the target class drops significantly, while only a small drop in performance is observed for non-target classes. This indicates a heavy reliance on class-exclusive, non-shared weights in the feature detectors. Interestingly, Csordás et al. (2020) also shows the mis-classification behaviors based on "shared features" (or possibly spurious features), e.g., when "airplane" is removed, images are often misclassified as "birds" or "ships," both of which commonly feature a blue background.

Zhang et al. (2021) investigates the capability of finding a subnetwork for a specific task within a trained dense network by extracting it using a specially designed held-out dataset tailored for that task. Specifically, the authors train a dense network on the Colored MNIST dataset, which contains a high spurious correlation between digits and colors, with each digit being strongly correlated with a particular color. Using the same technique as Csordás et al. (2020), but while pruning, Zhang et al. (2021) trains the network with a dataset balanced in terms of colors and digits to isolate subnetworks that solely predict either digits or colors. Surprisingly, even though the trained dense network suffers significantly from spurious correlations, it is still possible to extract a subnetwork that predicts only the digits with high accuracy, without extensive retraining on a balanced (or non-spurious) dataset.

Park et al. (2023) constructs the mask training data by upweighting the complex cases (called by bias-conflict samples) defined by the misclassified cases of the ERM model, aiming to extract a set of weights more robust to those cases therefore, eliminating bias in the network.

A.3 Multiple spurious attributes

CelebA - Dataset contains multiple spurious attributes. We analyze 7 chosen attributes having annotations from dataset, namely: male, no beard, heavy makeup, wearing lipstick, young, pale skin, big nose. Treating each attribute independently, we show their potential of being spurious attribute by comparing the worst-group accuracy from set $\mathcal{G} = \{(\text{blond}, a_i), (\text{non-blond}, a_i), (\text{blond}, \text{non-}a_i), (\text{non-blond}, \text{non-}a_i)\}$ for each attribute a_i and the ERM average accuracy. A fair model should treat all groups equally and minimize the influence of distribution. As shown in Tab. 9 (cf. ERM), we see some gaps between worst-group and average accuracy, and at the same time the unequal accuracy among groups.

Model performance across multiple spurious attributes. Tab. 9 shows more details on the accuracies of each group and compares among more methods; namely ERM, DCWP, GroupDRO, DFR, and Ours. Interestingly, when considering the group having the worst performance by ERM, our method outperforms

all others by considerable margins. We argue that our cluster sampling stage can find hard cases even more effectively than methods using ERM failures such as DCWP.

Table 9: Details of group accuracy (%) with respect to multiple attributes in CelebA dataset. Average accuracy of baseline ResNet18 is 89.4%. After pruning, our subnetwork has keep_ratio 45.5% of ResNet18 weights. We color the column corresponding to the minority group with respect to the combination of target and spurious attribute.

	T = Blond_hair	{T=0, A=0}	{T=0, A=1}	{T=1, A=0}	{T=1, A=1}
Male	ERM	78.5	98.9	98.9	50.2
	DCWP	75.9	92.7	97.0	81.8
	Ours	90.5	90.8	89.6	91.2
	GroupDRO	88.5	91.1	93.5	88.8
	DFR	84.9	85.6	94.9	85.6
No_Beard	ERM	99.4	85.7	37.5	96.7
	DCWP	93.9	81.6	78.1	96.4
	Ours	92.3	89.6	92.2	89.7
	GroupDRO	95.8	89.1	85.9	94.9
	DFR	90.4	82.4	78.1	96.6
Heavy_Makeup	ERM	92.6	79.6	88.9	99.3
	DCWP	87.4	76.9	92.7	97.8
	Ours	88.9	92.7	89.2	89.9
	GroupDRO	89.4	90.6	91.5	94.1
	DFR	84.4	83.1	93.8	97.6
Wearing_Lipstick	ERM	94.6	79.4	82.1	99.1
	DCWP	88.9	76.9	90.0	97.5
	Ours	88.7	92.2	89.8	89.7
	GroupDRO	89.6	89.9	90.0	94.0
	DFR	84.9	82.6	91.8	97.4
Young	ERM	90.9	87.5	92.1	96.7
	DCWP	84.7	83.7	95.3	96.3
	Ours	81.4	92.8	94.1	88.8
	GroupDRO	84.5	91.3	95.1	92.9
	DFR	79.1	85.4	96.0	96.4
Pale_Skin	ERM	88.5	83.5	95.8	97.9
	DCWP	84.1	79.2	96.2	95.2
	Ours	90.2	88.7	89.6	90.6
	GroupDRO	89.8	87.5	93.3	92.7
	DFR	84.0	81.9	96.4	96.1
Big_Nose	ERM	85.8	95.3	96.7	86.9
	DCWP	81.3	91.4	96.2	94.4
	Ours	90.4	89.4	89.4	93.3
	GroupDRO	89.2	91.3	93.1	94.7
	DFR	82.8	87.2	96.3	96.9

A.4 Feature Visualization

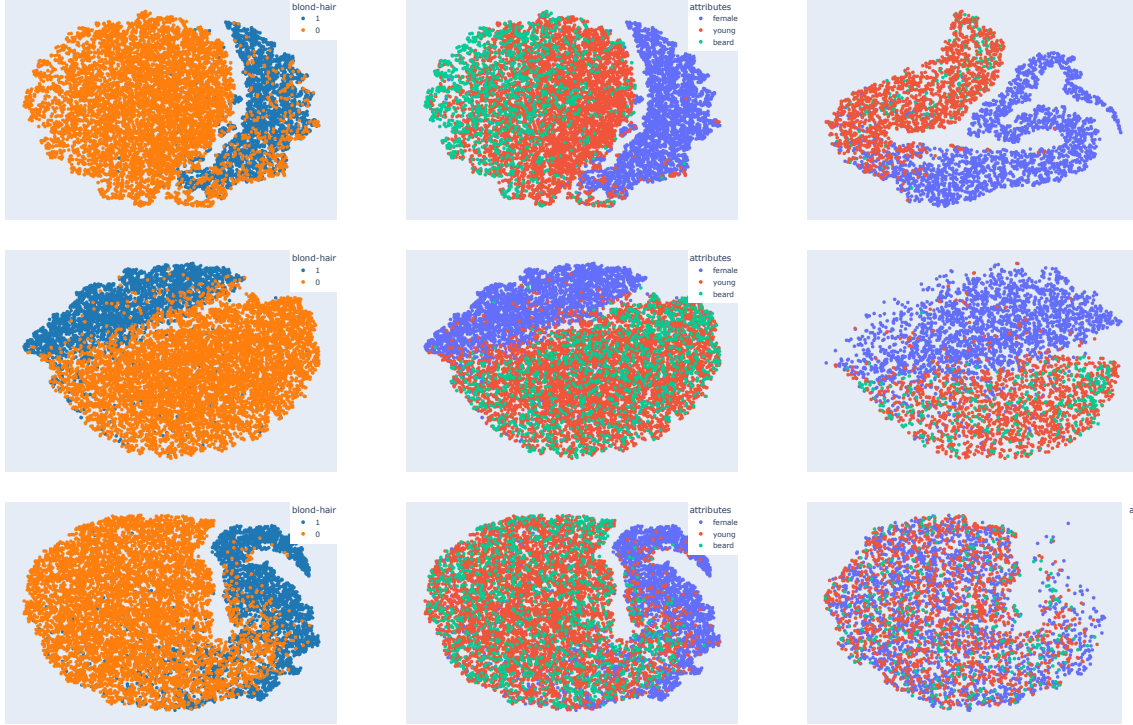


Figure 6: Embedding space of ERM (first row), DCWP (second row), and our pruned network (third row) on CelebA for predicting blond hair color. We visualize the train set embedding space with colors representing the class of non-blond hair (left column) and three other attributes: female, young, and beard (center column). To show how the approach works on test set, we visualize the class non-blond hair of test set, coloring above spurious attributes (right column). In both train and test embedding, ERM clusters well spurious attributes even those attribute labels are not used during training; showing its priority to learn spurious features. DCWP leveraging the ERM-misclassified cases can not mitigate the influence of attribute *female*, shown by a high purity cluster of samples with attribute *female* in both train and test representation space. Our pruned model mixes up samples in the same class, eliminating the biased learning behavior.